Nanoscale

Accepted Manuscript

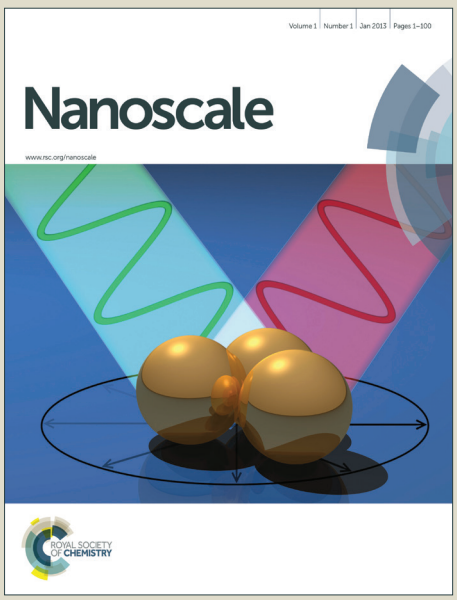

ROYAL SOCIETY OF CHEMISTRY

www.rsc.org/nanoscale

Nanoscale

RSCPublishing

COMMUNICATION

Nanoalloying bulk-immiscible iridium and palladium inhibits hydride formation and promotes catalytic performances

Cite this: DOI: 10.1039/x0xx00000x

Received 00th January 2012,
Accepted 00th January 2012

DOI: 10.1039/x0xx00000x

www.rsc.org/

C. Zlotea,[a] F.Morfin,[b] T.S. Nguyen,[b] N.T. Nguyen,[c] J. Nelayah,[c] C. Ricolleau,[c] M. Latroche[a] and L.Piccolo*[b]

The hydrogen sorption properties of oxide-supported Ir-Pd nanoalloys have been determined for the first time, and correlated with their catalytic behavior. The addition of Ir to Pd suppresses hydride formation and leads to improved catalytic performances with respect to pure metals in the preferential oxidation of CO in H_2 excess (PROX).

Nanosizing metal particles can dramatically change their physical and hydrogen absorption properties. This strategy has recently emerged as an effective way to improve the kinetic and thermodynamic properties of hydrogen-storage materials.[1,2] Due to the presence of a significant fraction of surface atoms and the small solid-state core, the surface-mediated processes and the diffusion of hydrogen throughout the core are greatly enhanced by nanosizing.[3] Beside hydrogen storage, these effects can play an important role in catalysis. Indeed, noble metal/alloy nanoparticles supported on high-surface-area oxides constitute one of the most important classes of solid catalysts, and hydrogen is involved in many industrially-relevant reactions.[4] When hydrogen is absorbed in the nanoparticles, it modifies the active phase, which may have, depending on the reaction, promoting or detrimental effects on the catalytic performances.[5–9] In order to design more efficient catalysts, it is therefore crucial to understand the interplay between hydrogen absorption and catalytic properties of metal nanoparticles.

Among all noble metals, palladium is both an important catalytic metal and the only bulk metal which forms a hydride phase ($PdH_{0.7}$) at ambient temperature and pressure.[10–14] Therefore, it has become the most studied metal-hydrogen system for highlighting nanosize effects.[15–17] Decreasing the Pd particle size increases the hydrogen absorption rate,[18] decreases the metal-hydrogen mixing enthalpy/entropy and critical temperature,[19] and reversibly changes the lattice structure.[20] Moreover, the absorption capacity at a given pressure diminishes when decreasing the size.[15,21]

Other noble metals exhibit extremely low hydrogen solubility in the bulk crystal phase at ambient pressure due to their endothermic reaction with hydrogen.[22] However, for nanometric sizes, the significant contribution of the surface energy term to the overall energy of the nanoparticles is expected to change the hydrogen absorption properties of non-absorbing bulk metals. The surface energy term may contribute as an induced additional pressure term increasingly important when reducing the size. Indeed, nanosize-induced hydrogen absorption in Rh and Ir nanoparticles stabilized into PVP polymers has been recently reported.[23,24] Both materials can absorb a small amount of hydrogen and form solid solutions at ambient temperature and pressure.

Along with nanosizing, nanoalloying between/with non-absorbing noble elements is also expected to change the hydrogen absorption properties. Hydrogen absorption was reported for nanoalloys of two non-absorbing and bulk-immiscible elements: Ag and Rh.[25] For Pd-Au nanoalloys, the hydrogen uptake drastically decreases when increasing the Au content.[26] Pd-Pt nanoalloys absorb more hydrogen than pure Pd for a Pt concentration up to 21 at.% but further increase in Pt concentration has a negative effect on the absorption capacity,[27] in good agreement with recent DFT calculations.[28] Recently, bulk-immiscible Pd-Ru nanoalloys were reported to exhibit change from exothermic to endothermic reaction with hydrogen when increasing the Ru content.[29] This results in a strong reduction of absorbed hydrogen from 0.6 to 0.08 H/M from pure Pd to $Pd_{0.5}Ru_{0.5}$ at 26 °C. However, all these works were performed with unsupported and PVP-protected nanoparticles, which are generally not suitable for practical catalysis.

The bulk-immiscible Ir-Pd system has been only scarcely studied in the past,[30–32] and its hydrogen sorption (absorption and/or adsorption) properties are unknown. However, it has been recently shown that supported Ir-Pd nanoparticles could act as efficient catalysts, [33–36] in particular for the preferential

oxidation of CO in the presence of excess H_2 (PROX).[36] This reaction is important for purifying H_2 before using it as a fuel in PEM fuel cells. In this communication, we show that the superior performances of supported Ir-Pd nanoalloys with respect to their Ir or Pd counterparts are related to the fact that the nanoalloys absorb significantly less hydrogen.

Three catalysts were prepared by incipient wetness (co)impregnation of amorphous silica-alumina (ASA) with $Ir(acac)_3$ or(and) $Pd(acac)_2$ dissolved in toluene. ASA is a mildly acidic mesoporous solid (BET surface area *ca.* 500 $m^2 g^{-1}$) widely used in heterogeneous catalysis.[37] The metal-acetylacetonate precursors were then decomposed by heating the samples up to 550 °C in a hydrogen flow (see ESI for experimental details). With such a reducing treatment, metal agglomeration was avoided and the final catalysts were free of carbonaceous residues.[35,38] The metal loadings were determined by ICP-OES to be 2.5 wt.% for Ir/ASA, 0.89 wt.% for Pd/ASA, and 4.5 wt.% for Ir-Pd/ASA. The mean atomic composition of the Ir-Pd sample was $Ir_{49}Pd_{51}$ (noted IrPd later on).

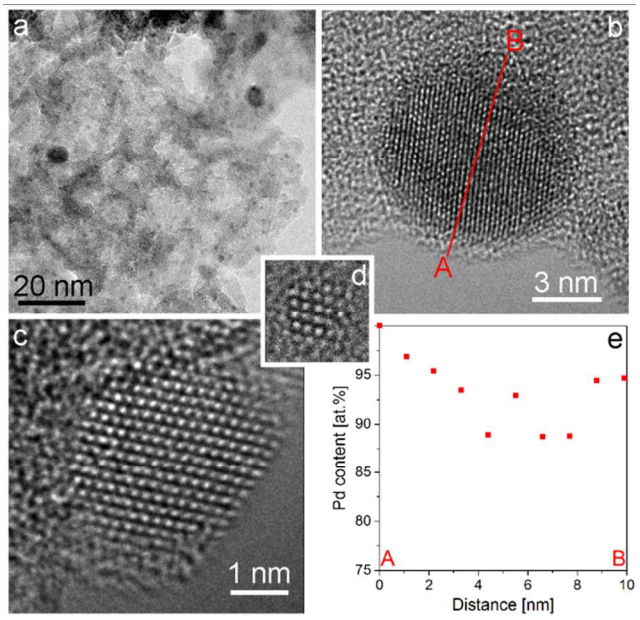

Figure 1. TEM investigation of the IrPd/ASA catalyst. *a* Low-magnification view of a collection of particles. *b-d* Aberration-free high-resolution images of a 10 nm-sized particle (*b*), a 4 nm-sized particle (*c*), and a 1 nm-sized particle (*d*, same scale as *c*). (*e*) EDX linescan of the particle in *b*.

The catalyst structure was investigated by powder X-ray diffraction (XRD), aberration-corrected transmission electron microscopy (TEM), and energy dispersive X-ray (EDX) spectroscopy. TEM observations (Fig. 1) confirm and supplement a previous investigation of similar systems supported on ASA and γ-Al_2O_3.[35,36] The surface-averaged nanoparticle sizes for Ir, Pd, and IrPd samples are 1.5 ± 0.3 nm, 4.5 ± 1.2 nm, and 2.2 ± 0.8 nm, respectively. For the IrPd sample, a small fraction of Pd-enriched defective particles larger than 6 nm was also observed (Fig. 1a) due to the aggregation induced by the high metal loading needed for absorption measurements on poorly absorbing catalysts (i.e., Ir-containing ones). However, the sorption results (see below) show that the influence of these Pd-rich particles is negligible. The metal dispersion was further checked by oxygen chemisorption measurements (see details in ESI). The mean diameters obtained with this method are 1.7 nm (Ir), 4.7 nm (Pd) and 2.2 nm (IrPd), in excellent agreement with the TEM results.

EDX analyses showed bimetallic particles exhibiting size-composition correlation, the Pd content increasing with the particle size (Fig. S3). Consistently, at the bottom and top ends of the size distribution, small Ir-rich (Fig. 1*d*) and large Pd-rich particles (Fig. 1*b*) were present. It was previously demonstrated that, although often neglected in the literature, size-dependent particle composition is a general phenomenon inherent to bimetallic catalyst preparation methods.[31] Similar to nanoparticle size dispersion for metallic catalysts prepared by conventional impregnation, it cannot be avoided if a thermal treatment is involved, since it is due to metal-dependent Ostwald ripening.[39] TEM observations such as those reported in Figure 1(*b-d*) showed no indication of segregated (core-shell, Janus…) or ordered structure, suggesting the presence of homogeneous random nanoalloys. However, spatially resolved EDX showed the presence of Pd surface enrichment for the biggest particles (Fig. 1*e*). The mean composition ($Ir_{49}Pd_{51}$) and the size-composition correlation were uniform throughout the surface of the support, and are fully consistent with previous results for low-loaded samples (0.9 wt% metal).[35]

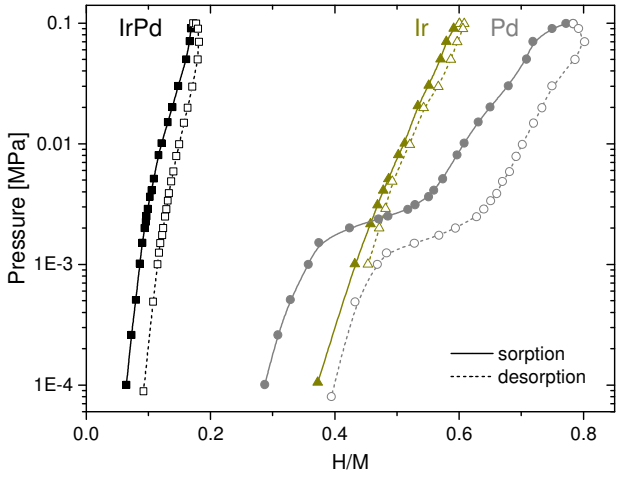

Figure 2. Pressure-composition isotherms at RT for ASA-supported nanoparticles (protocol I, see text). H/M stands for the number ratio between sorbed hydrogen atoms and metal atoms.

Hydrogen sorption properties were determined by measuring the pressure-composition isotherms (PCI) at RT (25 °C) up to 0.1 MPa hydrogen pressure using an automated volumetric device (see protocol I in ESI for details). A pretreatment was performed before the measurements: the catalysts were reduced

in H_2 atmosphere at 120 °C, and then desorbed under secondary vacuum at the same temperature. Note that this treatment was intended not only to reduce the metals but also to saturate the surface sites with chemisorbed hydrogen without preventing hydrogen absorption (see below).[40] The hydrogen sorption properties of the ASA support were determined and no obvious sorption/desorption was observed up to 0.1 MPa. Therefore, the sorption behaviors of the three supported metal catalysts can be entirely attributed to metal nanoparticle-induced processes.

The PCI curves for the three samples are shown in Figure 2. The sorption and desorption are reversible for all samples in the present conditions. The PCI curve for Pd/ASA clearly shows the presence of a sloppy plateau pressure with large absorption/desorption hysteresis. This indicates the formation at low pressure of a Pd(H) solid solution, which converts into a hydride phase PdH_x on the plateau, in good agreement with the literature.[15] The maximum hydrogen sorption capacities in the solid solution and the hydride phase are 0.36 H/M (at 1.5 kPa) and 0.78 H/M (at 0.1 MPa), respectively. These values are higher than usually reported for 5 nm-sized Pd nanoparticles (0.10 and 0.65 H/M, respectively).[41] In the present case, other hydrogen sorption phenomena might take place at low pressure: (i) hydrogen consumption by reduction of surface metal oxides;[42] (ii) hydrogen adsorption (physisorption and/or chemisorption) on surface sites; (iii) hydrogen spillover from the metal nanoparticles to the support.[43]
The former hypothesis (i) can be excluded since the preconditioning of the samples was sufficient to reduce any surface oxide possibly present on the nanoparticles. Moreover, the good repeatability of the measurements (ESI) clearly proves that the investigated nanoparticles were in metallic state.
To check the second hypothesis (ii), a series of additional H_2 sorption experiments was performed on the three catalysts following a procedure similar to that used for oxygen chemisorption measurements (hydrogen sorption protocol II, see ESI). The low working temperature (30 °C) favored Pd hydride formation and allowed us to compare the results with the data of Fig. 2 (protocol I). Reversible (physisorption and absorption) and irreversible (surface chemisorption) contributions were extracted. At variance from the pretreatment temperature applied in protocol I (120 °C), a treatment at 300 °C under secondary vacuum was carried out in order to completely remove adsorbed hydrogen before each sorption measurement. The pressure vs. H/M curves obtained from these experiments (Fig. 3 and Fig. S8) confirm the behavior exhibited by the PCI curves in Fig. 2, *provided that the contribution of chemisorption is removed*. Consistent with our experiments, nuclear reaction analysis experiments have demonstrated that chemisorbed hydrogen saturates the surface of Pd nanoparticles (size ca. 2 nm) at very low pressure (6 10^{-4} Pa) and fully desorbs above 200 °C.[40] Therefore, using our protocol I, chemisorbed hydrogen was always present at the surface of the metal particles (without blocking absorption), i.e., surface chemisorption of hydrogen had no significant contribution in the PCI measurements. Hence, the elevated H/M values measured for supported Pd and Ir particles at around 100 Pa do not originate from surface chemisorption. Nevertheless, H_2 physisorption cannot be excluded.
Finally, hydrogen spillover (iii) might take place at low pressure, before absorption. Spillover is an important effect in heterogeneous catalysis.[44] At low pressure, the H_2 molecules dissociate (via a physisorbed state) at the metal surface and either remain chemisorbed at the metal surface or are spilt over the support surface surrounding the particles, leading to an enhancement of the total hydrogen capacity.
For both Ir and IrPd samples, no plateau pressure is observed, indicating the formation of solid solutions with increasing hydrogen concentration as pressure increases. This result is in agreement with the formation of a hydrogen solid solution in 1.5 nm-sized Ir nanoparticles immobilized in PVP recently reported by Kobayashi et. al.[24] However, in our case, the capacity of Ir is 0.60 H/M at 0.1 MPa, which is much higher than the value of 0.18 H/M reported by Kobayashi et. al.24. Similarly to the case of Pd/ASA, a spillover effect might occur at low pressure for Ir/ASA, increasing the overall hydrogen capacity.

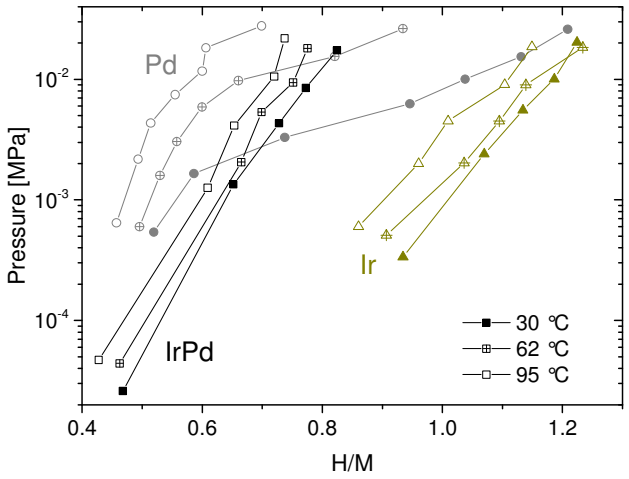

Figure 3. Pressure-composition isotherms at three temperatures for ASA-supported nanoparticles (protocol II, first isotherm, see text and ESI).

If both Ir and Pd nanoparticles can accommodate hydrogen, Ir-Pd nanoalloys could behave as an intermediate sorption system between nanosized Ir and Pd. However, the sorption behavior of IrPd is different, showing an almost suppressed contribution at low pressure. The maximum hydrogen sorption capacity of supported Ir-Pd nanoalloys (0.18 H/M at 0.1 MPa) and the hydrogen solubility in the whole pressure range considered (from 10^{-4} to 0.1 MPa) are much lower than those of both Ir and Pd nanoparticles under same pressure conditions (Fig. 2). This result corroborates previous findings showing a drastic decrease of the hydrogen uptake for PVP-embedded $Pd_{50}Au_{50}$ (0.03 H/M at 0.1 MPa),[26] $Pd_{50}Pt_{50}$ (0.17 H/M at 0.1 MPa) [27] and $Pd_{50}Ru_{50}$ (0.08 H/M at 0.1 MPa) [29] with respect to Pd. Both Pt and Au elements are located close to Ir in the periodic table and therefore may exhibit similar electronic and structural effects

when alloyed with Pd. Recent DFT calculations performed on Pd-Pt nanoalloys have shown that, for a Pt content approaching 50 at.%, the hydrogen insertion energy increases to values exceeding those for pure Pd.[28] The explanation proposed is based on structural aspects: the available volumes for hydrogen insertion decrease for a Pt content approaching 50 at.%, and hydrogen absorption generates strong anisotropic internal distortions. The Ir-Pd nanoalloy structure may be unfavorable to hydrogen absorption as well. Moreover, the chemisorption of H_2 at the nanoalloy surface might be inhibited at low pressure, preventing hydrogen spillover.

In order to investigate further the sorption properties of Ir-Pd nanoalloys as compared to Ir and Pd ones, protocol II was applied not only at 30 °C but also at 62 °C and 95 °C. The curves for Ir and IrPd, which have essentially no inflexion point at 30 °C, exhibit one at higher temperature (Fig. 3 and Fig. S8), suggesting an endothermic metal-H reaction. Moreover, the pressure value of this inflexion decreases as temperature increases, at variance from the Pd behavior. This means that, when adding Ir to Pd in similar amounts, the hydrogen sorption behavior switches from exothermic to endothermic, just like in the case of Pd-Ru nanoalloys.[29]

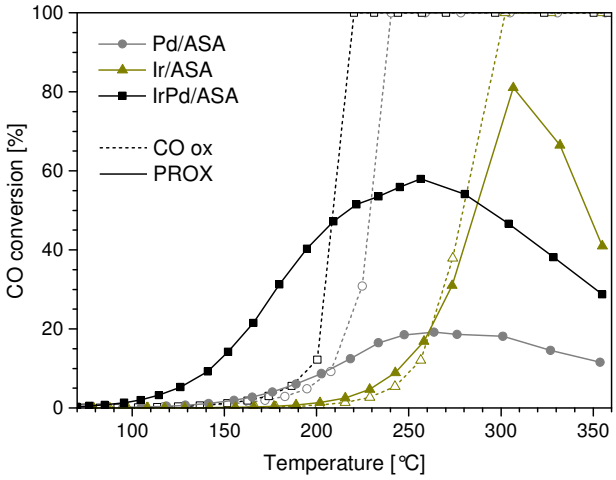

Figure 4. Catalytic performances of supported nanoparticles in CO oxidation and PROX.

The strikingly different hydrogen sorption behavior of supported Ir-Pd nanoparticles with respect to that of Ir and Pd particles, and the corresponding differences in electronic structures due to the formation of a solid-solution alloy, are expected to have important consequences on the catalyst performances under hydrogen atmosphere. Figure 4 shows the results of CO conversion during CO oxidation (flow of 2% CO and 2% O_2 in He, 1 atm) and CO PROX (*idem* with 48% H_2) on the three catalysts. Although Pd is a very efficient H_2-free CO oxidation catalyst (the Pd turnover frequency is two orders of magnitude higher than that of Ir around 150 °C, see Fig. S10), it is the least CO_2-selective of all the platinum-group metals in PROX.[45,46] Conversely, Ir is highly selective but poorly active (Fig. S11). Noticeably, at low temperature, the IrPd catalyst is both more active and selective in PROX than the Ir and Pd catalysts. Consistently, only the IrPd activity is boosted by the presence of H_2, with a decrease of the light-off temperature by more than 50 °C (turnover frequency multiplied by 11 at 150 °C). The present results confirm previous experiments performed on low-metal-loaded catalysts, where $Ir_{89}Pd_{11}$ and $Ir_{55}Pd_{45}$ nanoalloys have been found more active and selective than their Ir-pure or Pd-rich counterparts (or mechanical Ir + Pd mixtures) in PROX, independently of the support (ASA or alumina).[36]

From PROX experiments on ceria-supported Pd and Pt catalysts and *in situ* XPS experiments, Pozdnyakova *et al.* ascribed the poor catalytic performances of Pd to hydride formation.[47] Indeed, it suppressed the possibility of CO oxidation due to the preferential reaction of oxygen with hydride hydrogen to form water. The present H sorption results, showing that Ir-Pd nanoparticles sorb ca. 3 and 6 times less hydrogen than Ir and Pd ones, respectively (Fig. 2 at RT and 50 kPa), may explain the promotional effect of Ir-Pd alloying in PROX. Ir-Pd nanoparticles retain the high activity of Pd in H_2-free CO+O reaction oxidation while preventing bulk hydrogen dissolution and hydride formation, which is detrimental to PROX. In support to sorption-PROX correlations, it should be noted that chemisorbed CO has a minor blocking effect on hydrogen absorption by high-surface-area palladium.[48]

Conclusions

Our results confirm hydrogen absorption in Pd nanoparticles (solid solution and hydride) as well as nanosize-induced hydrogen absorption into a non-absorbing element, Ir (solid solution), in the case of supported catalysts. Moreover, the overall hydrogen sorption capacity decreases strongly for Ir-Pd nanoalloys as compared to pure Ir and Pd nanoparticles. The addition of Ir to Pd inhibits Pd hydride formation, and the supported Ir-Pd nanoparticles adopt an endothermic behavior toward reaction with hydrogen. The nanoalloying effect on hydrogen sorption is shown for the first time to correlate with a synergistic effect in a catalytic reaction involving hydrogen.

Acknowledgements

The authors from IRCELYON and MPQ acknowledge the French government for funding under the ANR DINAMIC BS10-009 project. The authors from IRCELYON thank M. Aouine & L. Burel for additional TEM observations, and N. Cristin & P. Mascunan for ICP analyses. The authors from MPQ acknowledge the Ile-de-France Region for SESAME E1845 convention supporting the Jeol ARM 200F electron microscope installed at the Paris-Diderot University. The French GDR CNRS 3182 "Nanoalliages" and the European "Nanoalloy" COST Action MP0903 are acknowledged for stimulating collaborations.

Notes and references

[a] ICMPE, Institut de Chimie et des Matériaux de Paris-Est, UMR 7182 CNRS & Université Paris Est Créteil, 2-8 rue Henri Dunant, 94320 Thiais, France.
[b] IRCELYON, Institut de recherches sur la catalyse et l'environnement de Lyon, UMR 5256 CNRS & Université Claude Bernard - Lyon 1, 2 avenue Albert Einstein, 69626 VILLEURBANNE CEDEX, France.
[c] MPQ, Laboratoire Matériaux et Phénomènes Quantiques, UMR 7162 CNRS & Université Paris-Diderot, Bâtiment Condorcet, 4 rue Elsa Morante, 75205 Paris Cedex 13, France.

Electronic Supplementary Information (ESI) available: Detailed catalyst preparation procedure, additional TEM-EDX results, XRD data, and additional sorption and catalysis results. See DOI: 10.1039/c000000x/

1. Q. Zhang, E. Uchaker, S. L. Candelaria, and G. Cao, *Chem. Soc. Rev.*, 2013, **42**, 3127.
2. P. E. de Jongh, M. Allendorf, J. J. Vajo, and C. Zlotea, *MRS Bull.*, 2013, **38**, 488–494.
3. P. E. de Jongh and P. Adelhelm, *ChemSusChem*, 2010, **3**, 1332–1348.
4. I. Chorkendorff and J. W. Niemantsverdriet, *Concepts of Modern Catalysis and Kinetics*, Wiley-VCH, Weinheim, 2nd edn., 2007.
5. Z. Paál, *Hydrogen effects in catalysis: fundamentals and practical applications*, M. Dekker, New York, 1988.
6. D. Teschner, J. Borsodi, A. Wootsch, Z. Revay, M. Havecker, A. Knop-Gericke, S. D. Jackson, and R. Schlogl, *Science*, 2008, **320**, 86–89.
7. M. Armbrüster, M. Behrens, F. Cinquini, K. Föttinger, Y. Grin, A. Haghofer, B. Klötzer, A. Knop-Gericke, H. Lorenz, A. Ota, S. Penner, J. Prinz, C. Rameshan, Z. Révay, D. Rosenthal, G. Rupprechter, P. Sautet, R. Schlögl, L. Shao, L. Szentmiklósi, D. Teschner, D. Torres, R. Wagner, R. Widmer, and G. Wowsnick, *ChemCatChem*, 2012, **4**, 1048–1063.
8. A. Valcarcel, F. Morfin, and L. Piccolo, *J. Catal.*, 2009, **263**, 315–320.
9. L. Piccolo, in *Nanoalloys: Synthesis, Structure and Properties*, Springer-Verlag, London, D. Alloyeau, C. Mottet, C. Ricolleau (Eds.)., 2012.
10. D. N. Jewett and A. C. Makrides, *Trans. Faraday Soc.*, 1965, **61**, 932–939.
11. F. A. Lewis, *The Palladium-Hydrogen System*, New York, Academic., 1967.
12. F. A. Lewis, *Int. J. Hydrogen Energy*, 1996, **21**, 461–464.
13. E. Wicke, H. Brodowsky, and H. Züchner, in *Topics in Applied Physics*, New York, Springer., 1978, vol. 29, p. 73.
14. T. B. Flanagan and W. A. Oates, *Annu. Rev. Mater. Sci.*, 1991, **21**, 269–304.
15. A. Pundt and R. Kirchheim, *Annu. Rev. Mater. Res.*, 2006, **36**, 555–608.
16. M. Yamauchi, R. Ikeda, H. Kitagawa, and M. Takata, *J. Phys. Chem. C*, 2008, **112**, 3294–3299.
17. C. Zlotea and M. Latroche, *Colloids Surf. A*, 2013, **439**, 117.
18. C. Langhammer, V. P. Zhdanov, I. Zorić, and B. Kasemo, *Phys. Rev. Lett.*, 2010, **104**, 135502.
19. J. A. Eastman, L. J. Thompson, and B. J. Kestel, *Phys. Rev. B*, 1993, **48**, 84–92.
20. C. Zlotea, F. Cuevas, V. Paul-Boncour, E. Leroy, P. Dibandjo, R. Gadiou, C. Vix-Guterl, and M. Latroche, *J. Am. Chem. Soc.*, 2010, **132**, 7720–7729.
21. P. Dibandjo, C. Zlotea, R. Gadiou, C. Matei Ghimbeu, F. Cuevas, M. Latroche, E. Leroy, and C. Vix-Guterl, *Int. J. Hydrogen Energy*, 2013, **38**, 952–965.
22. A. Driessen, P. Sanger, H. Hemmes, R. Griessen, *J. Phys.: Condens. Matter* 1990, **2,** 9797-9814.
23. H. Kobayashi, H. Morita, M. Yamauchi, R. Ikeda, H. Kitagawa, Y. Kubota, K. Kato, and M. Takata, *J. Am. Chem. Soc.*, 2011, **133**, 11034–11037.
24. H. Kobayashi, M. Yamauchi, and H. Kitagawa, *J. Am. Chem. Soc.*, 2012, **134**, 6893–6895.
25. K. Kusada, M. Yamauchi, H. Kobayashi, H. Kitagawa, and Y. Kubota, *J. Am. Chem. Soc.*, 2010, **132**, 15896–15898.
26. H. Kobayashi, M. Yamauchi, R. Ikeda, and H. Kitagawa, *Chem. Commun.*, 2009, 4806–4808.
27. H. Kobayashi, M. Yamauchi, H. Kitagawa, Y. Kubota, K. Kato, and M. Takata, *J. Am. Chem. Soc.*, 2010, **132**, 5576–5577.
28. A. Lebon, A. García-Fuente, A. Vega, and F. Aguilera-Granja, *J. Phys. Chem. C*, 2012, **116**, 126–133.
29. K. Kusada, H. Kobayashi, R. Ikeda, Y. Kubota, M. Takata, S. Toh, T. Yamamoto, S. Matsumura, N. Sumi, K. Sato, K. Nagaoka, and H. Kitagawa, *J. Am. Chem. Soc.*, 2014, **136**, 1864–1871.
30. S. N. Tripathi, S. R. Bharadwaj, and M. S. Chandrasekharaiah, *J. Phase Equilib.*, 1991, **12**, 603–605.
31. P. E. A. Turchi, V. Drchal, and J. Kudrnovský, *Phys. Rev. B*, 2006, **74**, 064202.
32. B. Kolb, S. Müller, D. B. Botts, and G. L. W. Hart, *Phys. Rev. B*, 2006, **74**, 144206.
33. Y. M. López-De Jesús, C. E. Johnson, J. R. Monnier, and C. T. Williams, *Top. Catal.*, 2010, **53**, 1132–1137.
34. S. Y. Shen, T. S. Zhao, and J. B. Xu, *Electrochim. Acta*, 2010, **55**, 9179–9184.
35. L. Piccolo, S. Nassreddine, M. Aouine, C. Ulhaq, and C. Geantet, *J. Catal.*, 2012, **292**, 173–180.
36. F. Morfin, S. Nassreddine, J. L. Rousset, and L. Piccolo, *ACS Catal.*, 2012, **2**, 2161–2168.
37. S. Nassreddine, S. Casu, J. L. Zotin, C. Geantet, and L. Piccolo, *Catal. Sci. Technol.*, 2011, **1**, 408–412.
38. S. Nassreddine, G. Bergeret, B. Jouguet, C. Geantet, and L. Piccolo, *Phys. Chem. Chem. Phys.*, 2010, **12**, 7812–7820.
39. D. Alloyeau, G. Prévot, Y. Le Bouar, T. Oikawa, C. Langlois, A. Loiseau, and C. Ricolleau, *Phys. Rev. Lett.*, 2010, **105**, 255901.
40. M. Wilde, K. Fukutani, M. Naschitzki, and H.-J. Freund, *Phys. Rev. B*, 2008, **77**, 113412.
41. C. Sachs, A. Pundt, R. Kirchheim, M. Winter, M. T. Reetz, and D. Fritsch, *Phys. Rev. B*, 2001, **64**, 075408.
42. C. M. Ghimbeu, C. Zlotea, R. Gadiou, F. Cuevas, E. Leroy, M. Latroche, and C. Vix-Guterl, *J. Mater. Chem.*, 2011, **21**, 17765–17775.
43. G. M. Psofogiannakis and G. E. Froudakis, *Chem. Commun.*, 2011, **47**, 7933–7943.
44. G. M. Pajonk, *Appl. Catal. A*, 2000, **202**, 157–169.
45. S. H. Oh and R. M. Sinkevitch, *J. Catal.*, 1993, **142**, 254–262.
46. F. Mariño, C. Descorme, and D. Duprez, *Appl. Catal. B*, 2004, **54**, 59–66.
47. O. Pozdnyakova, D. Teschner, A. Wootsch, J. Kröhnert, B. Steinhauer, H. Sauer, L. Toth, F. C. Jentoft, A. Knop-Gericke, Z. Paál, and R. Schlögl, *J. Catal.*, 2006, **237**, 17–28.

48. T. B. Flanagan, D. Wang, K. L. Shanahan, *Phys. Chem. Chem. Phys.*, 2000, **2**, 4976-4982.

